A stabilized one–point integrated quadrilateral Reissner–Mindlin plate element

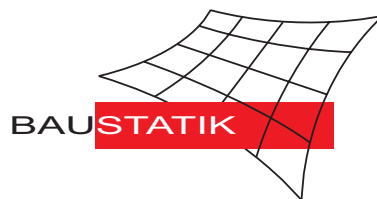**F. Gruttmann, W. Wagner**

BAUSTATIK

Universität Karlsruhe (TH)
Institut für Baustatik

A stabilized one–point integrated quadrilateral Reissner–Mindlin plate element

F. Gruttmann, W. Wagner

Mitteilung 7(2003)

BAUSTATIK

Prof. Dr.–Ing. W. Wagner
Institut für Baustatik
© Universität Karlsruhe
Postfach 6980
76128 Karlsruhe

Telefon: (0721) 608–2280
Telefax: (0721) 608–6015
E–mail: bs@.uni-karlsruhe.de
Internet: http://www.bs.uni-karlsruhe.de

A stabilized one–point integrated quadrilateral Reissner–Mindlin plate element

F. Gruttmann
Institut für Werkstoffe und Mechanik im Bauwesen
Technische Universität Darmstadt
Alexanderstraße 7
64283 Darmstadt
Germany

W. Wagner
Institut für Baustatik
Universität Karlsruhe (TH)
Kaiserstraße 12
76131 Karlsruhe
Germany

Contents

Abstract   A new quadrilateral Reissner–Mindlin plate element with 12 element degrees of freedom is presented. For linear isotropic elasticity a Hellinger–Reissner functional with independent displacements, rotations and stress resultants is used. Within the mixed formulation the stress resultants are interpolated using five parameters for the bending moments and four parameters for the shear forces. The hybrid element stiffness matrix resulting from the stationary condition can be integrated analytically. This leads to a part obtained by one point integration and a stabilization matrix. The element possesses a correct rank, does not show shear locking and is applicable for the evaluation of displacements and stress resultants within the whole range of thin and thick plates. The bending patch test is fulfilled and the computed numerical examples show that the convergence behaviour is better than comparable quadrilateral assumed strain elements.

Keywords: Hellinger–Reissner variational principle, quadrilateral element, effective analytical stiffness integration, one point integration plus stabilization matrix, bending patch test

1   Introduction

In the past, considerable research efforts have been directed towards the development of efficient and reliable finite plate elements and numerous publications can be found in the literature. For an overview on different plate formulations we refer e.g. to the textbook [1]. The so–called DKT and DKQ elements, where the Kirchhoff constraints are only fulfilled at discrete points, have been successfully applied for thin plates, e.g. [2]. Most of the work has been focussed on the Reissner–Mindlin model, [3, 4]. This by–passes the difficulties caused by C^1 requirements of the classical Kirchhoff theory [1, 5]. However, the standard bilinear interpolation for the transverse displacements and rotations leads to severe shear locking for thin plates. One method to avoid shear locking is the application of reduced integration or selective reduced integration, see e.g. [6, 7]. This leads to a rank deficiency of the element stiffness matrix and thus for certain boundary conditions to zero energy modes for the assembled system. Hence several authors have developed stabilization techniques to regain the correct rank of the element stiffness matrix, e.g. [8, 9]. These techniques have been extended and refined for different boundary value problems in [10], where stabilization matrices on basis of the enhanced strain method have been derived. A further method uses substitute shear strain fields [11], subsequently extended and reformulated in [12, 13] and [14, 15, 16]. In [17] the authors propose procedures to impose shear strain fields which satisfy a priori the conditions of vanishing transverse shear strains for the thin plate limit. A Taylor series expansion of the stiffness is derived using an assumed strain interpolation in [18]. The DST and DSQ elements can be seen as further developments of the discrete Kirchhoff elements, now with incorporation of the transverse shear strains at discrete points, e.g. [19]. For mixed hybrid models the choice of assumed internal stress fields is particularly crucial, e.g. [20, 21, 22].

The essential features and novel aspects of the present formulation are as follows:
The element possesses a correct rank with three zero eigenvalues corresponding to the three

rigid body modes of a plate. It fulfills the bending patch test for constant bending moments and leads due to the analytical integration of the matrices to a fast stiffness computation. The paper is organized as follows. The variational formulation for a linear plate accounting for transverse shear strains is based on a Hellinger-Reissner functional. Hence the finite element matrices are given. The interpolation functions for the displacements, strains and stress resultants are specified. Explicit expressions for the element matrices are derived. The analytical integration leads to the element stiffness matrix which is obtained by one-point integration plus a stabilization matrix. No parameters have to be adjusted to avoid locking or to prevent hourglass modes. Several examples demonstrate the efficiency of the developed finite plate element.

2 Basic Equations

2.1 Variational Formulation

In this section the basic equations of a Reissner–Mindlin plate theory are summarized. We denote the domain of the plate by Ω, the boundary by Γ and the thickness by h. The plate is loaded by transverse load $\bar{\mathbf{p}} = [p, 0, 0]^T$ in Ω and by boundary loads $\bar{\mathbf{t}} = [\bar{p}, \bar{m}_x, \bar{m}_y]^T$ on Γ_σ. The variational formulation is based on a Hellinger–Reissner functional, where the displacement field and the stress resultants are independent quantities.

$$\Pi_{HR}(\mathbf{u}, \boldsymbol{\sigma}) = \int_{(\Omega)} (\boldsymbol{\varepsilon}^T \boldsymbol{\sigma} - \frac{1}{2} \boldsymbol{\sigma}^T \mathbf{C}^{-1} \boldsymbol{\sigma}) \, dA - \int_{(\Omega)} \mathbf{u}^T \bar{\mathbf{p}} \, dA - \int_{(\Gamma_\sigma)} \mathbf{u}^T \bar{\mathbf{t}} \, ds \quad \rightarrow \quad \text{stat.} \quad (1)$$

Here, the displacement field is denoted by $\mathbf{u} = [w, \beta_x, \beta_y]^T$, where w is the transverse deflection, β_x and β_y the rotations about y and x axes, see Fig. 1. Furthermore, we introduce the vector of stress resultants $\boldsymbol{\sigma} = [m_x, m_y, m_{xy}, q_x, q_y]^T$ with the bending moments m_x, m_y, m_{xy} and the shear forces q_x, q_y. The curvatures and the transverse shear strains are organized in a vector as follows

$$\boldsymbol{\varepsilon} = \begin{bmatrix} \kappa_x \\ \kappa_y \\ 2\kappa_{xy} \\ \gamma_x \\ \gamma_y \end{bmatrix} = \begin{bmatrix} \beta_{x,x} \\ \beta_{y,y} \\ \beta_{x,y} + \beta_{y,x} \\ \beta_x + w_{,x} \\ \beta_y + w_{,y} \end{bmatrix}. \quad (2)$$

Furthermore, the constitutive matrix for linear isotropic elasticity is introduced as

$$\mathbf{C} = \begin{bmatrix} \mathbf{C}^b & \mathbf{0} \\ \mathbf{0} & \mathbf{C}^s \end{bmatrix} \quad \text{with} \quad \mathbf{C}^b = D \begin{bmatrix} 1 & \nu & 0 \\ \nu & 1 & 0 \\ 0 & 0 & \frac{1-\nu}{2} \end{bmatrix}, \quad \mathbf{C}^s = \kappa\, G\, h \begin{bmatrix} 1 & 0 \\ 0 & 1 \end{bmatrix} \quad (3)$$

with the bending rigidity $D = \frac{Eh^3}{12\,(1-\nu^2)}$, Young´s modulus E, shear modulus G, Poisson´s ratio ν and shear correction factor $\kappa = \frac{5}{6}$.
The stationary condition yields

$$\delta\Pi_{HR}(\mathbf{u}, \boldsymbol{\sigma}, \delta\mathbf{u}, \delta\boldsymbol{\sigma}) = \int_{(\Omega)} [\delta\boldsymbol{\varepsilon}^T \boldsymbol{\sigma} + \delta\boldsymbol{\sigma}^T (\boldsymbol{\varepsilon} - \mathbf{C}^{-1}\boldsymbol{\sigma}) - \delta\mathbf{u}^T \bar{\mathbf{p}}] \, dA - \int_{(\Gamma_\sigma)} \delta\mathbf{u}^T \bar{\mathbf{t}} \, ds = 0 \quad (4)$$

3

with virtual displacements $\delta\mathbf{u} = [\delta w, \delta\beta_x, \delta\beta_y]^T$ and virtual stresses $\delta\boldsymbol{\sigma} = [\delta m_x, \delta m_y, \delta m_{xy}, \delta q_x, \delta q_y]^T$.

2.2 Finite Element Equations

For a quadrilateral element we exploit the isoparametric concept with coordinates ξ and η defined in the unit square $\{\xi, \eta\} \in [-1, 1]$, see Fig. 1, and interpolate the transverse displacements and rotations using bilinear functions

$$w = \mathbf{N}^T \mathbf{w}, \quad \beta_x = \mathbf{N}^T \boldsymbol{\beta}_x, \quad \beta_y = \mathbf{N}^T \boldsymbol{\beta}_y. \tag{5}$$

Here, $\mathbf{w}$, $\boldsymbol{\beta}_x$, $\boldsymbol{\beta}_y$ denote the nodal displacements and rotations and $\mathbf{N}$ the vector of the bilinear shape functions

$$\mathbf{N} = [N_1, N_2, N_3, N_4]^T = \mathbf{a}_0 + \xi\,\mathbf{a}_1 + \eta\,\mathbf{a}_2 + \xi\eta\,\mathbf{h}$$

$$\mathbf{a}_0 = \frac{1}{4}\begin{bmatrix} 1 \\ 1 \\ 1 \\ 1 \end{bmatrix} \qquad \mathbf{a}_1 = \frac{1}{4}\begin{bmatrix} -1 \\ 1 \\ 1 \\ -1 \end{bmatrix} \qquad \mathbf{a}_2 = \frac{1}{4}\begin{bmatrix} -1 \\ -1 \\ 1 \\ 1 \end{bmatrix} \qquad \mathbf{h} = \frac{1}{4}\begin{bmatrix} 1 \\ -1 \\ 1 \\ -1 \end{bmatrix}. \tag{6}$$

For the virtual displacements the same interpolation functions are used.

The fulfillment of the bending patch test is discussed in appendix A, see also Taylor et al. [23]. There it is shown, that with the transverse shear strains emanating from the Reissner–Mindlin kinematic the bending patch test can not be fulfilled within the present mixed formulation. The non constant part of the shear strains according to (2) leads for a constant stress state to a contribution of the shear energy on the element level.

For this reason we approximate the shear strains with independent interpolation functions proposed in [14] as follows

Figure 1: Quadrilateral plate element

$$\begin{bmatrix} \gamma_x \\ \gamma_y \end{bmatrix} = \mathbf{J}^{-1} \begin{bmatrix} \gamma_\xi \\ \gamma_\eta \end{bmatrix} \quad \text{where} \quad \begin{aligned} \gamma_\xi &= \frac{1}{2}[(1-\eta)\gamma_\xi^B + (1+\eta)\gamma_\xi^D] \\ \gamma_\eta &= \frac{1}{2}[(1-\xi)\gamma_\eta^A + (1+\xi)\gamma_\eta^C] \end{aligned} \tag{7}$$

4

with the Jacobian matrix computed with the nodal coordinates $\mathbf{x} = [x_1, x_2, x_3, x_4]^T$ and $\mathbf{y} = [y_1, y_2, y_3, y_4]^T$

$$\mathbf{J} = \begin{bmatrix} x_{,\xi} & y_{,\xi} \\ x_{,\eta} & y_{,\eta} \end{bmatrix} = \begin{bmatrix} \mathbf{x}^T (\mathbf{a}_1 + \eta \mathbf{h}) & \mathbf{y}^T (\mathbf{a}_1 + \eta \mathbf{h}) \\ \mathbf{x}^T (\mathbf{a}_2 + \xi \mathbf{h}) & \mathbf{y}^T (\mathbf{a}_2 + \xi \mathbf{h}) \end{bmatrix}. \tag{8}$$

Thus, with eq. (7) the covariant components of the shear strains are transformed to the cartesian coordinate system. The determinant yields

$$\begin{aligned} \det \mathbf{J} &= j_0 + \xi \, j_1 + \eta \, j_2 \\ j_0 &= (\mathbf{x}^T \mathbf{a}_1)(\mathbf{y}^T \mathbf{a}_2) - (\mathbf{x}^T \mathbf{a}_2)(\mathbf{y}^T \mathbf{a}_1) \\ j_1 &= (\mathbf{x}^T \mathbf{a}_1)(\mathbf{y}^T \mathbf{h}) - (\mathbf{y}^T \mathbf{a}_1)(\mathbf{x}^T \mathbf{h}) \\ j_2 &= (\mathbf{y}^T \mathbf{a}_2)(\mathbf{x}^T \mathbf{h}) - (\mathbf{x}^T \mathbf{a}_2)(\mathbf{y}^T \mathbf{h}). \end{aligned} \tag{9}$$

The strains at the midside nodes A, B, C, D, see Fig. 1 are specified as follows

$$\begin{aligned} \gamma_\xi^M &= [x_{,\xi} \, \beta_x + y_{,\xi} \, \beta_y + w_{,\xi}]^M & M &= B, D \\ \gamma_\eta^L &= [x_{,\eta} \, \beta_x + y_{,\eta} \, \beta_y + w_{,\eta}]^L & L &= A, C \end{aligned} \tag{10}$$

where the following quantities are given with the bilinear interpolation (5)

$$\begin{aligned} \beta_\alpha^A &= \tfrac{1}{2} (\beta_{\alpha 4} + \beta_{\alpha 1}) & \alpha &= x, y \\ \beta_\alpha^B &= \tfrac{1}{2} (\beta_{\alpha 1} + \beta_{\alpha 2}) \\ \beta_\alpha^C &= \tfrac{1}{2} (\beta_{\alpha 2} + \beta_{\alpha 3}) \\ \beta_\alpha^D &= \tfrac{1}{2} (\beta_{\alpha 3} + \beta_{\alpha 4}) \\ w_{,\eta}^A &= \tfrac{1}{2} (w_4 - w_1) \\ w_{,\xi}^B &= \tfrac{1}{2} (w_2 - w_1) \\ w_{,\eta}^C &= \tfrac{1}{2} (w_3 - w_2) \\ w_{,\xi}^D &= \tfrac{1}{2} (w_3 - w_4) \\ \mathbf{r}_{,\eta}^A &= \tfrac{1}{2} (\mathbf{r}_4 - \mathbf{r}_1) & \mathbf{r} &= \begin{bmatrix} x \\ y \end{bmatrix} \\ \mathbf{r}_{,\xi}^B &= \tfrac{1}{2} (\mathbf{r}_2 - \mathbf{r}_1) \\ \mathbf{r}_{,\eta}^C &= \tfrac{1}{2} (\mathbf{r}_3 - \mathbf{r}_2) \\ \mathbf{r}_{,\xi}^D &= \tfrac{1}{2} (\mathbf{r}_3 - \mathbf{r}_4) \end{aligned} \tag{11}$$

Remark:
An alternative three field variational formulation based on a Hu–Washizu principle for the shear part, which would be the appropriate variational formulation for an independent shear interpolation according to (7), leads to identical finite element matrices due to the fact that the shear stiffness matrix is diagonal.

Considering (2) and (5) - (11) the approximation of the strains is now obtained by

$$\varepsilon^h = \mathbf{B} \, \mathbf{v}, \qquad \mathbf{B} = [\mathbf{B}_1, \mathbf{B}_2, \mathbf{B}_3, \mathbf{B}_4], \qquad \mathbf{v} = [\mathbf{v}_1, \mathbf{v}_2, \mathbf{v}_3, \mathbf{v}_4]^T, \tag{12}$$

where $\mathbf{v}_I = [w_I, \beta_{xI}, \beta_{yI}]^T$ and the submatrices for bending and shear

$$\mathbf{B}_I = \begin{bmatrix} \mathbf{B}_I^b \\ \mathbf{B}_I^s \end{bmatrix}, \quad \mathbf{B}_I^b = \begin{bmatrix} 0 & N_{I,x} & 0 \\ 0 & 0 & N_{I,y} \\ 0 & N_{I,y} & N_{I,x} \end{bmatrix}, \quad \mathbf{B}_I^s = \mathbf{J}^{-1} \begin{bmatrix} N_{I,\xi} & b_I^{11} N_{I,\xi} & b_I^{12} N_{I,\xi} \\ N_{I,\eta} & b_I^{21} N_{I,\eta} & b_I^{22} N_{I,\eta} \end{bmatrix} \quad (13)$$

with

$$\begin{aligned}
b_I^{11} &= \xi_I \, x_{,\xi}^M & b_I^{12} &= \xi_I \, y_{,\xi}^M \\
b_I^{21} &= \eta_I \, x_{,\eta}^L & b_I^{22} &= \eta_I \, y_{,\eta}^L \, .
\end{aligned} \quad (14)$$

The coordinates of the unit square are $\xi_I \in \{-1, 1, 1, -1\}$, $\eta_I \in \{-1, -1, 1, 1\}$ and the allocation of the midside nodes to the corner nodes is given by $(I, M, L) \in \{(1, B, A); (2, B, C); (3, D, C); (4, D, A)\}$. The derivatives of the shape function $N_{I,x}$, $N_{I,y}$ are obtained in a standard way with the derivatives with respect to ξ, η and the inverse Jacobian matrix.

The stress field $\boldsymbol{\sigma}$ is interpolated as follows

$$\boldsymbol{\sigma}^h = \mathbf{S}\boldsymbol{\beta} \qquad \mathbf{S} = [\mathbf{1}_{(5\times 5)}, \tilde{\mathbf{S}}] \qquad \boldsymbol{\beta} = \left[\boldsymbol{\beta}^0, \boldsymbol{\beta}^1\right]^T$$

$$\tilde{\mathbf{S}} = \begin{bmatrix}
J_{11}^0 J_{11}^0 (\eta - \bar{\eta}) & J_{21}^0 J_{21}^0 (\xi - \bar{\xi}) & 0 & 0 \\
J_{12}^0 J_{12}^0 (\eta - \bar{\eta}) & J_{22}^0 J_{22}^0 (\xi - \bar{\xi}) & 0 & 0 \\
J_{11}^0 J_{12}^0 (\eta - \bar{\eta}) & J_{21}^0 J_{22}^0 (\xi - \bar{\xi}) & 0 & 0 \\
0 & 0 & J_{11}^0 (\eta - \bar{\eta}) & J_{21}^0 (\xi - \bar{\xi}) \\
0 & 0 & J_{12}^0 (\eta - \bar{\eta}) & J_{22}^0 (\xi - \bar{\xi})
\end{bmatrix}, \quad (15)$$

where the vectors $\boldsymbol{\beta}^0$ and $\boldsymbol{\beta}^1$ contain 5 and 4 parameters, respectively. The transformation coefficients $J_{\alpha\beta}^0$ in (15) denote the components of the Jacobian matrix (8) evaluated at the element center ($\xi = 0, \eta = 0$) and transform the contravariant components of the stress resultant tensors to the cartesian basis system. The coefficients have to be constant in order to fulfill the patch test, see Appendix A. The constants $\bar{\xi}$ and $\bar{\eta}$ which are introduced to obtain decoupled matrices denote the coordinates of the center of gravity of the element

$$\bar{\xi} = \frac{1}{A_e} \int\limits_{(\Omega_e)} \xi \, dA = \frac{1}{3} \frac{j_1}{j_0} \qquad \bar{\eta} = \frac{1}{A_e} \int\limits_{(\Omega_e)} \eta \, dA = \frac{1}{3} \frac{j_2}{j_0} \, . \quad (16)$$

The element area is given by $A_e = 4j_0$.

Remark:
The interpolation matrix for the stress resultants (15) is different to the procedure in [21], where 7 and 5 parameters are chosen for the bending and shear part, respectively. Thus a subsequent reduction of the number of parameters is necessary to obtain a stable element formulation. The interpolation of the bending moments in (15) corresponds to the approach of the Pian–Sumihara [24] hybrid quadrilateral with $\bar{\xi} = \bar{\eta} = 0$, see also the text book Zienkiewicz and Taylor, part 1, [1]. Finally we mention the paper of Baumann et al. [22], where the shear approximation is performed in a more complicated way.

Inserting (12) and (15) and the corresponding equations for the virtual stresses and virtual strains into the stationary condition (4) yields

$$\delta \Pi^h_{HR} = \sum_{e=1}^{numel} \begin{bmatrix} \delta\boldsymbol{\beta} \\ \delta\mathbf{v} \end{bmatrix}_e^T \left\{ \begin{bmatrix} -\mathbf{H} & \mathbf{G} \\ \mathbf{G}^T & \mathbf{0} \end{bmatrix} \begin{bmatrix} \boldsymbol{\beta} \\ \mathbf{v} \end{bmatrix} - \begin{bmatrix} \mathbf{0} \\ \mathbf{f} \end{bmatrix} \right\}_e = 0 \,, \tag{17}$$

where *numel* denotes the total number of plate elements to discretize the problem and the virtual element vectors $\delta\boldsymbol{\beta}$ and $\delta\mathbf{v}$, respectively. The element load vector $\mathbf{f} = [\mathbf{f}_1, \mathbf{f}_2, \mathbf{f}_3, \mathbf{f}_4]^T$ which follows from the external virtual work is identical with a pure displacement formulation. For a constant load p one obtains $\mathbf{f}_I = [f^w_I, 0, 0]^T$ with

$$f^w_I = A_e\, p \left(a_{0I} + \frac{1}{3}\frac{j_1}{j_0}a_{1I} + \frac{1}{3}\frac{j_2}{j_0}a_{2I}\right), \tag{18}$$

where a_{0I}, a_{1I}, a_{2I} are the components of the vectors defined in (6). The edge load $\bar{\mathbf{t}}$ leads to corresponding expressions.

Furthermore the matrices $\mathbf{H}$ and $\mathbf{G}$ are introduced

$$\mathbf{H} := \int_{(\Omega_e)} \mathbf{S}^T \mathbf{C}^{-1}\mathbf{S}\, dA\,, \qquad \mathbf{G} := \int_{(\Omega_e)} \mathbf{S}^T \mathbf{B}\, dA\,. \tag{19}$$

Since all integrants in (19) involve only polynomials of the coordinates ξ and η the integration for the element matrices can be carried out analytically. Due to the introduced constants $\bar{\xi}$ and $\bar{\eta}$ one obtains a decoupled matrix $\mathbf{H}$ as follows

$$\mathbf{H} = \begin{bmatrix} A_e\,\mathbf{C}^{-1} & \mathbf{0} \\ \mathbf{0} & \mathbf{h} \end{bmatrix} \qquad \text{with} \qquad \mathbf{h} = \begin{bmatrix} \mathbf{h}^b & \mathbf{0} \\ \mathbf{0} & \mathbf{h}^s \end{bmatrix}_{(4\times 4)}. \tag{20}$$

The components of the symmetric matrices $\mathbf{h}^b$ and $\mathbf{h}^s$ are given with

$$
\begin{aligned}
h^b_{11} &= \frac{4A_e f_{11}}{Eh^3}(J^{02}_{11} + J^{02}_{12})^2 \\
h^b_{22} &= \frac{4A_e f_{22}}{Eh^3}(J^{02}_{21} + J^{02}_{22})^2 \\
h^b_{12} &= h^b_{21} = \frac{4A_e f_{12}}{Eh^3}\left[(J^0_{11}\,J^0_{21} + J^0_{22}J^0_{12})^2 - \nu\,(J^0_{11}\,J^0_{22} - J^0_{12}J^0_{21})^2\right] \\
h^s_{11} &= \frac{A_e f_{11}}{3\kappa Gh}(J^{02}_{11} + J^{02}_{12}) \\
h^s_{22} &= \frac{A_e f_{22}}{3\kappa Gh}(J^{02}_{21} + J^{02}_{22}) \\
h^s_{12} &= h^s_{21} = \frac{A_e f_{12}}{3\kappa Gh}(J^0_{11}\,J^0_{21} + J^0_{22}J^0_{12})\,.
\end{aligned}
\tag{21}
$$

$$
\begin{aligned}
f_{11} &= 1 - \frac{1}{3}\left(\frac{j_2}{j_0}\right)^2 \\
f_{22} &= 1 - \frac{1}{3}\left(\frac{j_1}{j_0}\right)^2 \\
f_{12} &= -\frac{1}{3}\frac{j_1}{j_0}\frac{j_2}{j_0}
\end{aligned}
$$

Furthermore the matrix $\mathbf{G}$ is obtained by analytical integration as follows

$$\mathbf{G} = [\mathbf{G}_1, \mathbf{G}_2, \mathbf{G}_3, \mathbf{G}_4] \qquad \mathbf{G}_I = \begin{bmatrix} A_e\,\mathbf{B}_I^0 \\ \mathbf{g}_I \end{bmatrix} \qquad \mathbf{g}_I = \frac{1}{3}A_e\gamma_I \begin{bmatrix} 0 & J_{11}^0 & J_{12}^0 \\ 0 & J_{21}^0 & J_{22}^0 \\ 1 & \gamma_I^{11} & \gamma_I^{12} \\ 1 & \gamma_I^{21} & \gamma_I^{22} \end{bmatrix} \tag{22}$$

with $\mathbf{B}_I^0 = \mathbf{B}_I(\xi = 0, \eta = 0)$ and

$$\begin{aligned}
\gamma_I &= h_I - \frac{j_2}{j_0}a_{1I} - \frac{j_1}{j_0}a_{2I} \\
\gamma_I^{11} &= (b_I^{11}h_I - b_I^{11}\frac{j_2}{j_0}a_{1I} - b_I^{21}\frac{j_1}{j_0}a_{2I})/\gamma_I \\
\gamma_I^{12} &= (b_I^{12}h_I - b_I^{12}\frac{j_2}{j_0}a_{1I} - b_I^{22}\frac{j_1}{j_0}a_{2I})/\gamma_I \\
\gamma_I^{21} &= (b_I^{21}h_I - b_I^{11}\frac{j_2}{j_0}a_{1I} - b_I^{21}\frac{j_1}{j_0}a_{2I})/\gamma_I \\
\gamma_I^{22} &= (b_I^{22}h_I - b_I^{12}\frac{j_2}{j_0}a_{1I} - b_I^{22}\frac{j_1}{j_0}a_{2I})/\gamma_I \,.
\end{aligned} \tag{23}$$

The parameters h_I, a_{1I}, a_{2I} are the components of the nodal vectors defined in (6), whereas the quantities $b_I^{\alpha\beta}$ are defined in (14). Since the interpolation of the stress resultants are discontinuous at the element boundaries, the stress parameters are eliminated on element level

$$\boldsymbol{\beta} = \mathbf{H}^{-1}\mathbf{G}\,\mathbf{v}\,. \tag{24}$$

Thus considering (20) and (22) one obtains the element stiffness matrix

$$\begin{aligned}
\mathbf{k}^e &= \mathbf{G}^T\mathbf{H}^{-1}\mathbf{G} &= \mathbf{k}_0 + \mathbf{k}_{stab} \\
\mathbf{k}_{IK} &= \mathbf{G}_I^T\mathbf{H}^{-1}\mathbf{G}_K &= A_e\mathbf{B}_I^{0T}\mathbf{C}\mathbf{B}_K^0 + \mathbf{g}_I^T\mathbf{h}^{-1}\mathbf{g}_K\,.
\end{aligned} \tag{25}$$

Here, $\mathbf{k}_0$ denotes the stiffness matrix of a one–point integrated Reissner–Mindlin plate element with substitute shear strains and $\mathbf{k}_{stab}$ the stabilization matrix. An explicit representation of $\mathbf{k}_0$ is given in appendix B. The matrix $\mathbf{h}$ according to (20) consists of two submatrices of order two and thus can easily be inverted. The element possesses with three zero eigenvalues the correct rank.

3 Examples

The derived element formulation has been implemented in an extended version of the general purpose finite element program FEAP, see Zienkiewicz and Taylor [1]. For practical applications it is more convenient to introduce rotations θ_x, θ_y about the corresponding axes. Thus, the relations $\theta_x = -\beta_y$ and $\theta_y = \beta_x$ have been accounted for when setting up the element stiffness matrix, see Fig. 1. The other element formulations which have been considered for comparison have also been implemented in FEAP.

3.1 Constant bending patch test

First we investigate the element behaviour within a constant bending patch test as is depicted in Fig. 2. A rectangular plate of length a and width b supported at three corners is loaded by a concentrated load at the fourth corner and by bending moments at the corners. The geometrical and material data and the loading parameters are given. The solution of the problem can be computed analytically. The vertical displacement of node 1 is $w_1 = 12.48$ and the bending moments $m_x = m_y = m_{xy} = 1.0$ are constant throughout the plate.

Node	F_z	$\bar{m}_x$	$\bar{m}_y$
1	-2	20	-10
2	0	20	10
3	0	-20	10
4	0	-20	-10

$$
\begin{aligned}
a &= 40 \\
b &= 20 \\
h &= 0.1 \\
E &= 10^6 \\
\nu &= 0.3
\end{aligned}
$$
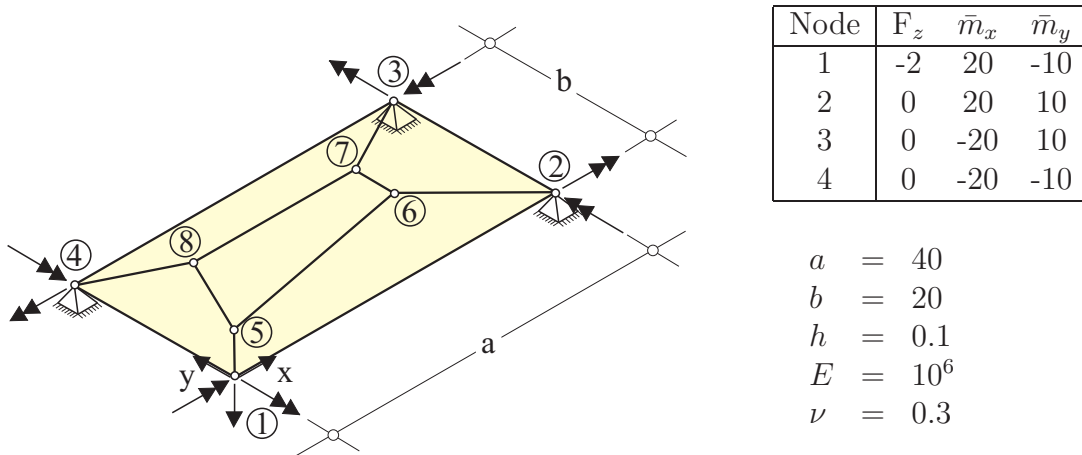
Figure 2: Rectangular plate, patch of 5 elements

The quadrilateral discrete Kirchhoff element [2] leads to the correct results. The results of the stabilized Belytschko/Tsay element [8] with parameters $r_w = 0.1$, $r_\beta = 0.05$ are presented in Fig. 3. The present element fulfills the patch test as Fig. 4 shows.

9
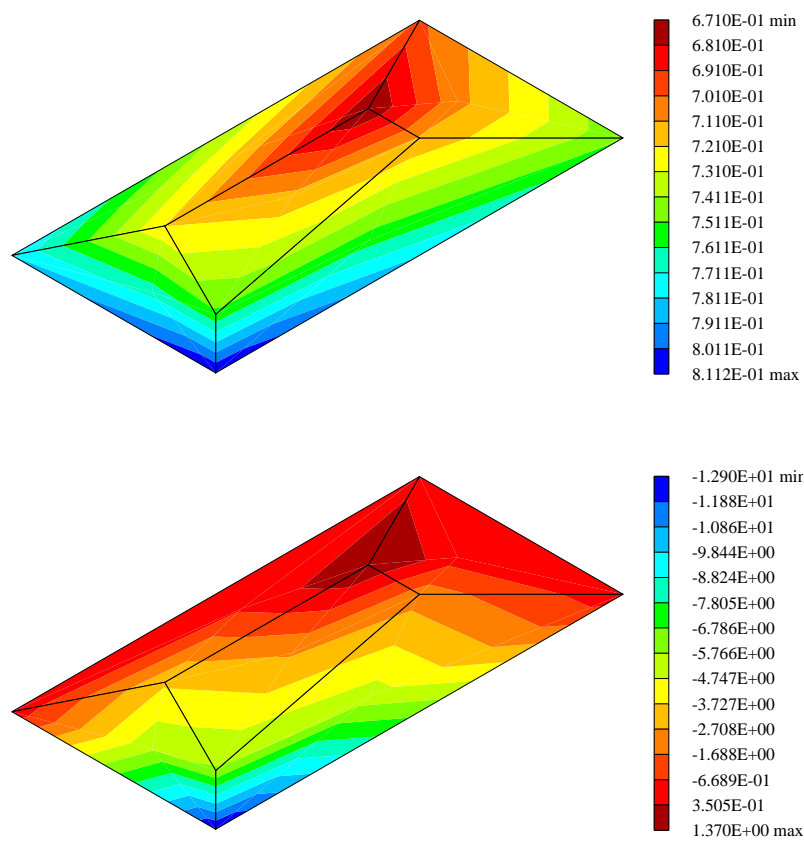
Figure 3: Moments m_x and displacements w for the Belytschko/Tsay element [8] with $r_w = 0.1$, $r_\beta = 0.05$
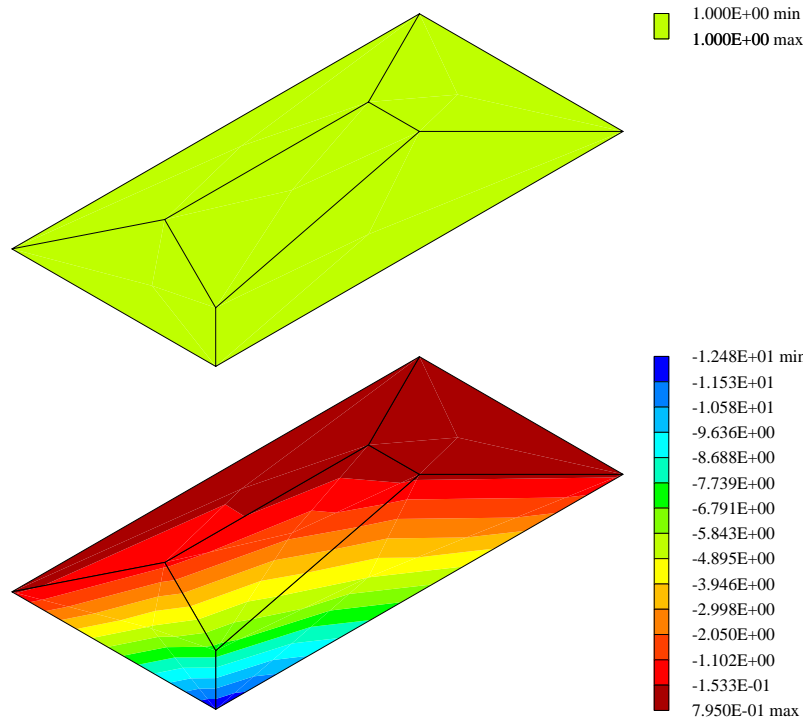
Figure 4: Moments m_x and displacements w for the present element

3.2 Square plate, test of mesh distorsion

3.2.1 Clamped square plate subjected to a concentrated load

$$
\begin{aligned}
a &= 100 \\
h &= 1 \\
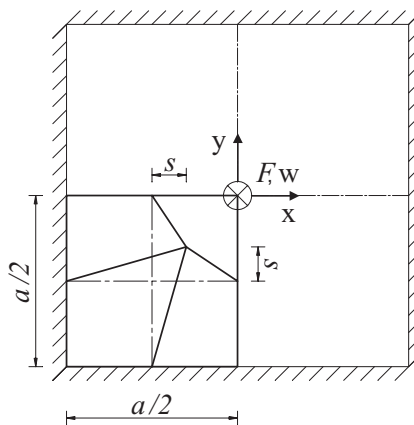F &= 16.3527 \\
E &= 10000 \\
\nu &= 0.3
\end{aligned}
$$

Figure 5: Distorted meshes for a clamped square plate subjected to a concentrated load

The problem with geometrical and material data is defined in Fig. 5. The mesh consists of 2×2 elements over a quarter of the plate, where fourfold symmetry has been used. Here the influence of element distorsion is tested, where one inner node is moved by $0 < s < 10$ in x- and y-direction. An analytical Kirchhoff solution for the center deflection yields $w = 0.0056\, Fa^2/D = 1$, see e.g. [5].

The sensitivity of the different element formulations with respect to the distorsion parameter s is depicted in Fig. 6. The DKQ–element [2] behaves relatively insensitive with respect to the mesh distorsion and yields for the present coarse mesh a solution which is too weak. The results computed with the new element are slightly better than with the Bathe/Dvorkin element [15]. The clamped plate allows a calculation without stabilization matrix, since the hourglass modes are suppressed by the boundary conditions. Thus for the present example the best results are obtained with the one point integrated element U_1. However this is not the case for arbitrary boundary conditions. Results for the Belytschko/Tsay element are similar to the element U_1 in the recommended range $0.02 \leq r_w \leq 0.05$. A contour plot of w with a distorsion parameter $s = 10$ is given in Fig. 7.
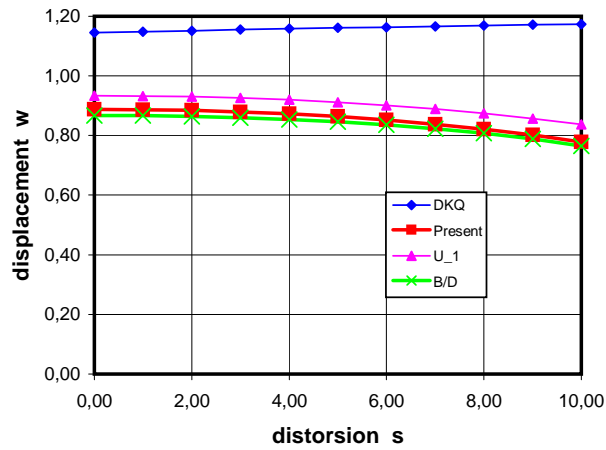
Figure 6: Influence of distorsion of FE-mesh on the center deflection of a clamped square plate subjected to a concentrated load
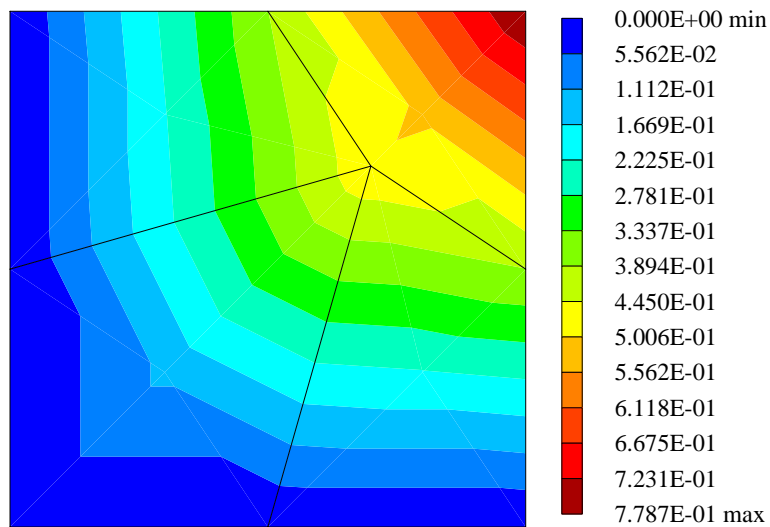

Figure 7: Displacements of a clamped square plate subjected to a concentrated load for the present element and a mesh distorsion s=10

3.2.2 Simply supported square plate subjected to uniform load

For this example the geometrical and material data have been taken from [21], see Fig. 8. Considering symmetry a quarter of the plate is discretized using 2×2 elements. Again distorted meshes are considered with a variation of the parameter $0 < s < 1$.

$$
\begin{aligned}
a &= 10 \\
h &= 0.01 \\
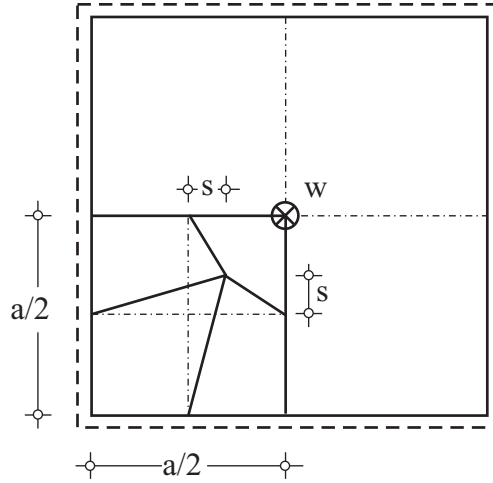q &= 10^{-3} \\
E &= 1092000 \\
\nu &= 0.3
\end{aligned}
$$

Figure 8: Distorted meshes for a simply supported square plate subjected to uniform load

Since the plate is rather thin a series solution based on the Kirchhoff theory can be taken for comparison, see e.g. [5]. The center deflection and the center moment are given as follows

$$
\begin{aligned}
w_{ref} &= w(\frac{a}{2}, \frac{a}{2}) = \frac{16\,q\,a^4}{\pi^6\,D} \sum_{m=1}^{\infty} \sum_{n=1}^{\infty} \frac{(-1)^{\frac{m+n}{2}-1}}{mn\,(m^2+n^2)^2} \\
m_{ref} &= m_x(\frac{a}{2}, \frac{a}{2}) = \frac{16\,q\,a^2}{\pi^4} \sum_{m=1}^{\infty} \sum_{n=1}^{\infty} \frac{(-1)^{\frac{m+n}{2}-1}}{mn\,(m^2+n^2)^2}(m^2+\nu n^2)\,.
\end{aligned}
\tag{26}
$$

Hence, evaluation of 15 series terms yields $w_{ref} = 0.40623$ and $m_{ref} = 0.004787$. These values are used to normalize the computed finite element results for distorsion parameters $s = 0$ and $s = 1$ in Table 1. The first row is taken from Table II of Ref. [21]. The results of the stabilized element [8] depend slightly on the choice of r_β for the stabilization of the rotations. Again, the present element shows a good behaviour among the considered four–node elements.

Element	w/w_{ref}(s=0)	m/m_{ref}(s=0)	w/w_{ref}(s=1)	m/m_{ref}(s=1)
HMPL5 [21]	-	-	1.030	0.940
B/D [15]	0.977	0.851	0.951	1.047
B/T [8] (0.0,0.02)	1.105	0.944	1.284	1.129
DKQ [2]	0.996	0.828	1.023	0.970
Present element	0.989	0.965	0.956	1.011

Table 1: Center deflection and moment

3.3 Square plate subjected to uniform load, test of convergence behaviour

This example is used to test the convergence behaviour of the presented element. A square plate subjected to uniform load and Navier boundary conditions is considered, see Fig. 9. Only one quarter of the plate is discretized due to fourfold symmetry.

$$
\begin{aligned}
a &= 10 \\
h &= 0.1 \\
q &= 1 \\
E &= 1092000 \\
\nu &= 0.3
\end{aligned}
$$
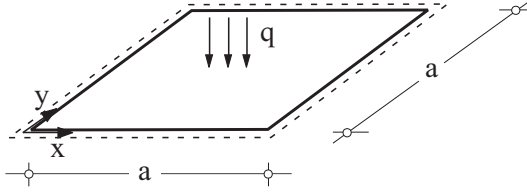
Figure 9: Square plate subjected to uniform load

The series solution of the Kirchhoff theory exploiting 15 series terms in eq. (26) yields $w(a/2, a/2) = 0.40623$, $m_x(a/2, a/2) = 4.787$. The finite element solutions also converge against the Kirchhoff solution since the shear deformations are suppressed with a large shear correction factor κ. The results for different mesh densities are presented in Table 2 in comparison to the discrete Kirchhoff element DKQ and the Bathe/Dvorkin element [15]. As can be seen the present element shows a superior convergence behaviour for the bending moment.

$w(a/2, a/2)$	1×1	2×2	4×4	8×8	16×16	32×32
DKQ	0.37903	0.40458	0.40600	0.40619	0.40622	0.40623
B/D ($\kappa = 1000$)	0.31888	0.39690	0.40414	0.40572	0.40611	0.40621
Present ($\kappa = 1000$)	0.33918	0.40177	0.40530	0.40601	0.40619	0.40623
analytical						0.40623

$m_x(a/2, a/2)$	1×1	2×2	4×4	8×8	16×16	32×32
DKQ	2.628	4.294	4.667	4.758	4.781	4.787
B/D ($\kappa = 1000$)	2.211	4.307	4.672	4.759	4.781	4.787
Present ($\kappa = 1000$)	2.998	4.619	4.751	4.779	4.786	4.787
analytical						4.787

Table 2: Convergence behaviour for center deflection and center moment m_x

3.4 Corner supported square plate

3.4.1 Load case 1: uniform load

A corner supported plate with edge length $2a$ subjected to uniform load is discussed. Considering symmetry the mesh consists of 8×8 elements for a quarter of the plate, see Fig. 10. The geometrical and material data are also given. An approximate ansatz according to [25] reads

$$
w(x, y) = c_1 + c_2 x^2 + c_3 y^2 + c_4 x^4 + c_5 x^2 y^2 + c_6 y^4 \,, \tag{27}
$$

where the origin of the co-ordinate system lies in the center of the plate. The boundary condition of vanishing bending moments at the edges can only be fulfilled in an integral sense. The other boundary conditions and the partial differential equation can be fulfilled exactly. The constants are determined and thus for $y = 0$ the approximate Kirchhoff solution reads

$$w(x, y = 0) = \frac{qa^4}{2Eh^3}[11 - 6\nu - \nu^2 + (-5 + 4\nu + \nu^2)(\frac{x}{a})^2 + (1 + \frac{\nu}{2} - \frac{\nu^2}{2})(\frac{x}{a})^4]. \quad (28)$$

$$\begin{aligned}
a &= 12 \\
h &= 0.375 \\
q &= 0.03125 \\
E &= 430000 \\
\nu &= 0.38 \\
\rho &= 0.001
\end{aligned}$$
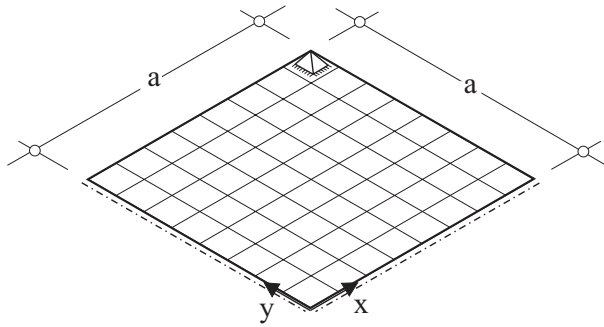
Figure 10: Corner supported plate

The deflections $w(x, y = 0)$ obtained with different elements are plotted in Fig. 11. The Belytschko/Tsay element [8] leads to hourglass modes for parameters $r_w < 0.02$, optimal results for $0.02 \leq r_w \leq 0.05$ and locking for $r_w > 0.05$, see also [8] and Fig. 11. The parameter $r_\beta = 0.02$ has been chosen constant in all cases.
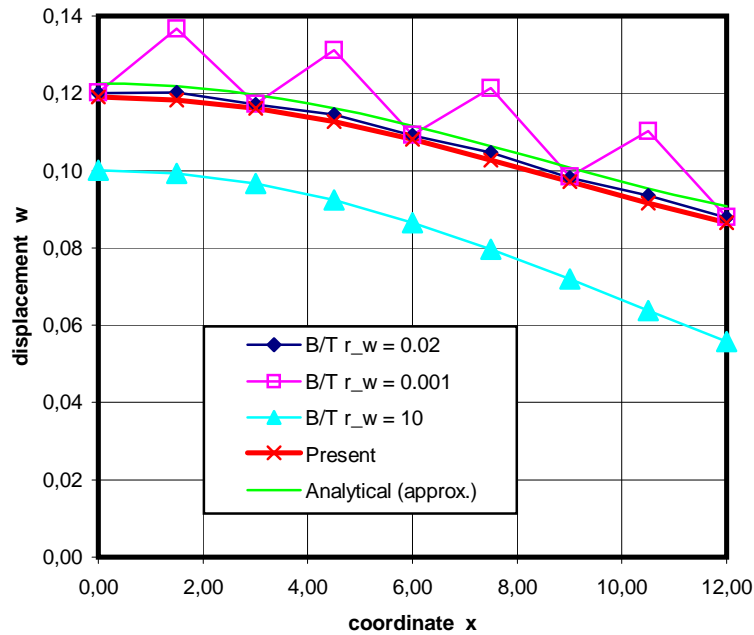

Figure 11: Deflection $w(x, y = 0)$ for the corner supported plate, comparison of different elements

15

The deformed mesh amplified by a factor 10 using the Belytschko/Tsay element with $r_w = 0.001$ and $r_\beta = 0.02$ is presented in Fig. 12. As can be seen for these parameters the hourglass modes can not be suppressed completely. Fig. 13 shows the amplified deformed mesh free of hourglassing and the associated contour plot using the present element.
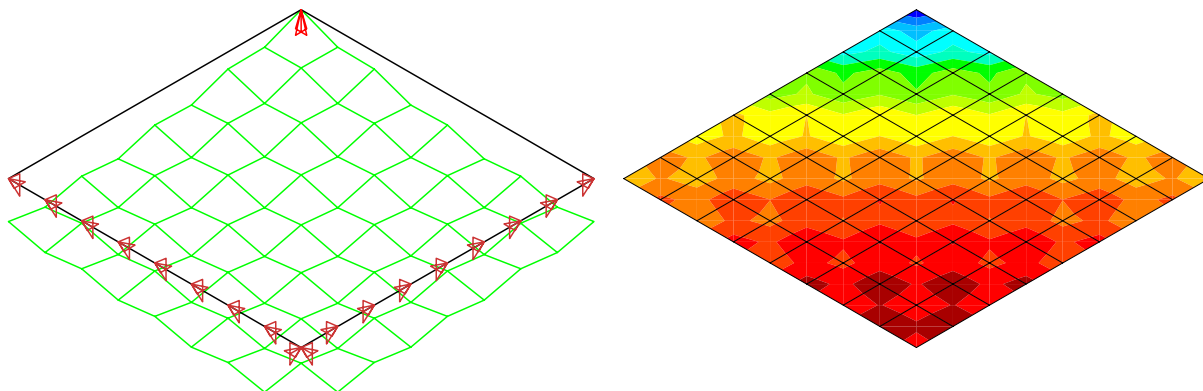

Figure 12: Deformed mesh for the corner supported plate, using the Belytschko/Tsay element with $r_w = 0.001$, $r_\beta = 0.02$
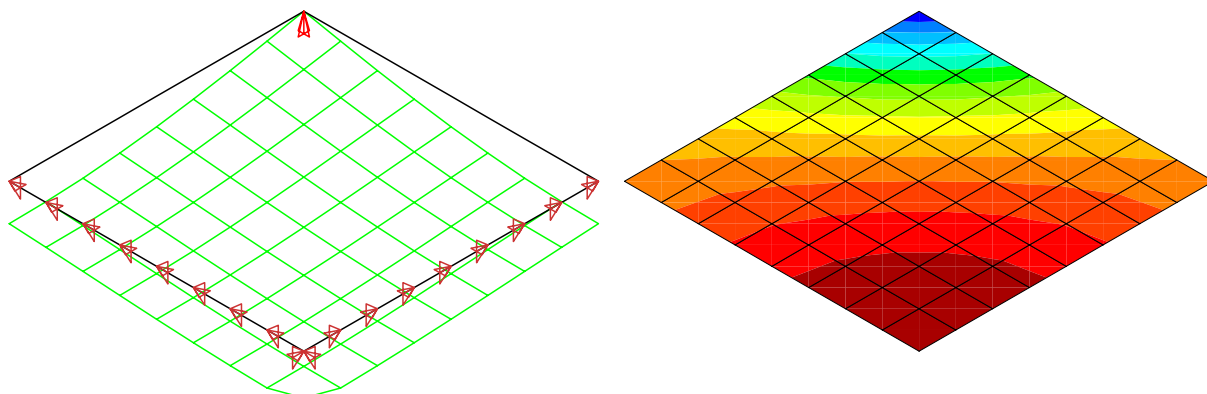

Figure 13: Deformed mesh for the corner supported plate, using the present element

For a convergence study of the center displacement the shear correction factor is again increased for the present element and the Bathe/Dvorkin element to approximate the Kirchhoff solution. The results according to Table 3 show nearly the same convergence behaviour for all three compared elements against the same value, which differs from the approximate analytical solution.

3.4.2 Load case 2: frequency analysis

Here the element behaviour is tested with a frequency analysis of the corner supported plate. Two mesh densities (6×6 and 96×96) are chosen for a quarter of the plate considering

	8×8	16×16	24×24	48×48	96×96	192×192
DKQ	0.11914	0.11960	0.11969	0.11974	0.11975	0.11976
B/D ($\kappa = 1000$)	0.11856	0.11946	0.11963	0.11973	0.11975	0.11976
Present ($\kappa = 1000$)	0.11862	0.11947	0.11963	0.11973	0.11975	0.11976
analytical (approx.)						0.12253

Table 3: Corner supported plate, convergence study

symmetry. Thus, only symmetric modes can be obtained. Within the eigenvalue analysis a consistent mass matrix has been used. The normalized frequencies $\bar{\omega} = \omega\,(2a)^2\,(D/\rho h)^{-1/2}$ are summarized for the different models in Table 4. The results of the fine mesh can be considered to be converged. An approximate analytical solution according to [26] is available. Solutions with the Belytschko/Tsay element show that a stabilization is necessary and that the results depend on the choice of the parameters r_w and r_β, see [8].

	6×6 mesh			96×96 mesh		
Element	$\bar{\omega}_1$	$\bar{\omega}_2$	$\bar{\omega}_3$	$\bar{\omega}_1$	$\bar{\omega}_2$	$\bar{\omega}_3$
B/T [8](0.03, 0.001)	7.054	18.789	43.279	7.028	18.647	43.124
B/D [15]	7.135	18.795	44.010	7.021	18.647	43.021
Present	7.131	18.794	43.961	7.021	18.647	43.020
DKQ [2]	7.117	18.750	43.998	7.073	18.656	43.538
Present($\kappa = 1000$)	7.144	18.800	44.105	7.073	18.656	43.537
analytical (approx.) [26]				7.120	19.600	44.400

Table 4: lowest frequencies for the corner supported square plate

From the results obtained with the fine mesh it can be seen that all Mindlin–type elements converge against the same solution. To compare with the Kirchhoff solution a further computation with $\kappa = 1000$ is performed. Finally the associated eigenvectors are depicted in Fig. 14
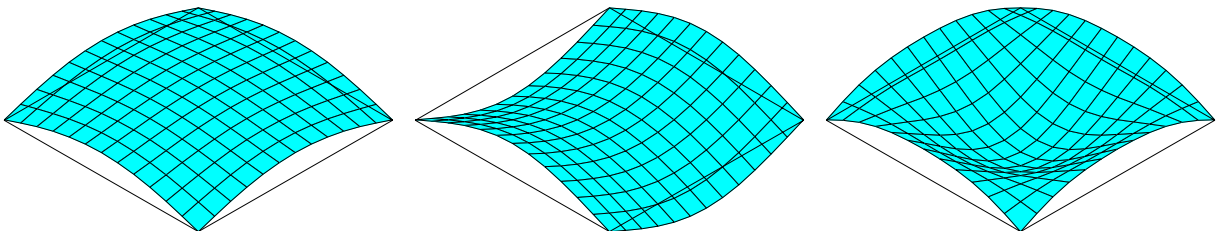

Figure 14: First three eigenvectors for the corner supported square plate

3.5 Clamped circular thick plate subjected to a concentrated load

As last example a thick clamped circular plate with Radius R subjected to a concentrated load F is considered, see also [8]. The problem with geometrical and material data is defined

17

in Fig. 15. The mesh consists of 3 blocks of 4×4 elements for a quarter of the plate, where fourfold symmetry has been used. The analytical solution considering shear deformations yields, see [3],[7]

$$w(r) = \frac{FR^2}{16\pi D}\left[(1 - \frac{r^2}{R^2}) + \frac{2r^2}{R^2}\ln\frac{r}{R} - \frac{8D}{\kappa GhR^2}\ln\frac{r}{R}\right]. \tag{29}$$

The last term describes the influence of the shear deformations and leads to unbounded displacements w at the center of the plate. The other terms are bounded and correspond to the Kirchhoff solution.

$$
\begin{aligned}
R &= 5 \\
h &= 2 \\
F &= 1 \\
E &= 1000 \\
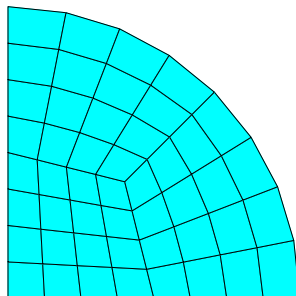\nu &= 0
\end{aligned}
$$

Figure 15: Clamped thick circular plate subjected to concentrated load

Results using different elements and an analytical solution (for $r/R \geq 0.002$) are plotted in Fig. 16. The deflections obtained with the DKQ element [2] are close to the Kirchhoff solution. Solutions calculated with the Belytschko/Tsay element [8] lead to a dependency on the parameters $r_w = r_\beta$. A standard Reissner–Mindlin element with full integration (SRI 2/2) tends for the present thick plate not to shear locking. The present element, the Belytschko/Tsay element (with $r_w = 0.1$), the Bathe/Dvorkin element and the SRI-element (2/2) lead to results which practically coincide with the analytical solution.

4 Conclusions

The formulation of a quadrilateral plate element with three displacement degrees of freedom (transverse displacement, two rotations) at each node has been presented. The element possesses a correct rank, does not show shear locking and is applicable for the evaluation of displacements and stress resultants within the whole range of thin and thick plates. No parameters have to be adjusted to avoid shear locking or to prevent zero energy modes. The investigations showed that the constant bending patch test is fulfilled. The computed results obtained for simply supported, clamped and corner supported plates with different load cases are very satisfactory. This holds for the calculated displacements and stress resultants and for the frequency analysis of plates. The convergence behaviour for the displacements and stresses is slightly better than comparable quadrilateral assumed strain elements. However the essential advantage is the fast stiffness computation due to the analytically derived stiffness.
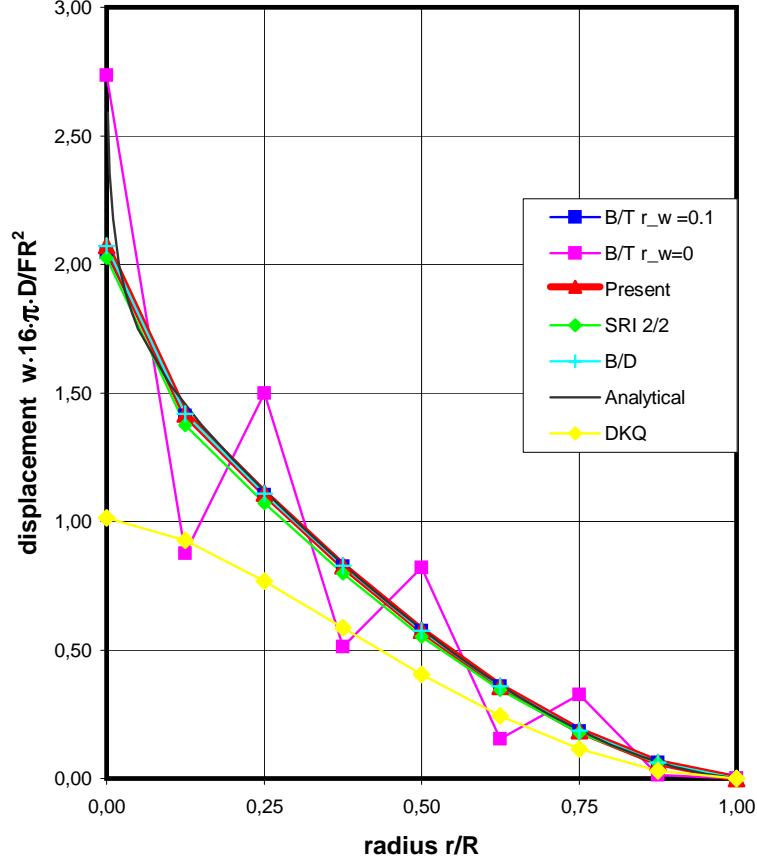
Figure 16: Displacements $w(r)$ for a clamped thick circular plate subjected to a concentrated load

A   Appendix, The bending patch test

For an arbitrary patch of elements and linear elasticity the constant stress state is considered

$$\boldsymbol{\sigma}^h = \mathbf{S}\,\boldsymbol{\beta} = \boldsymbol{\beta}^0 + \tilde{\mathbf{S}}\,\boldsymbol{\beta}^1 \quad = \quad \text{constant}\,. \tag{30}$$

Thus, the parameter vector $\boldsymbol{\beta}^1$ which refers to the non–constant part of the element stresses must vanish, $\boldsymbol{\beta}^1 = \mathbf{0}$. Next, eq. (24) is rewritten as

$$\begin{bmatrix} \boldsymbol{\beta}^0 \\ \boldsymbol{\beta}^1 \end{bmatrix} = \begin{bmatrix} \dfrac{1}{A_e}\mathbf{C} & \mathbf{0} \\ \mathbf{0} & \mathbf{h}^{-1} \end{bmatrix} \begin{bmatrix} \displaystyle\int_{(\Omega_e)} \mathbf{B}\,dA\,\mathbf{v} \\ \displaystyle\int_{(\Omega_e)} \tilde{\mathbf{S}}^T\mathbf{B}\,dA\,\mathbf{v} \end{bmatrix}. \tag{31}$$

We proceed with the second equation in (31) and obtain

$$\boldsymbol{\beta}^1 \quad = \quad \mathbf{h}^{-1} \int_{(\Omega_e)} \tilde{\mathbf{S}}^T \mathbf{B}\,dA\,\mathbf{v} = \mathbf{0} \tag{32}$$

Since $\mathbf{h}^{-1}$ is a positive definite matrix with linear independent shape functions for the stresses,

eq. (32) leads with $\boldsymbol{\varepsilon}^h = \mathbf{B}\mathbf{v} = \text{constant}$ to

$$\int\limits_{(\Omega_e)} \tilde{\mathbf{S}}^T \, dA = \mathbf{0} \,, \tag{33}$$

which is only fulfilled with constant coefficients $J^0_{\alpha\beta}$ in (15).

The finite element approximation of the strains (2) reads with (5)

$$\boldsymbol{\varepsilon}^h = \mathbf{B}\,\mathbf{v} \,, \qquad\qquad \mathbf{B} = [\mathbf{B}_1, \mathbf{B}_2, \mathbf{B}_3, \mathbf{B}_4] \,,$$

$$\mathbf{B}_I = \begin{bmatrix} \mathbf{B}^b_I \\ \mathbf{B}^s_I \end{bmatrix} \,, \qquad \mathbf{B}^b_I = \begin{bmatrix} 0 & N_{I,x} & 0 \\ 0 & 0 & N_{I,y} \\ 0 & N_{I,y} & N_{I,x} \end{bmatrix} \,, \qquad \mathbf{B}^s_I = \begin{bmatrix} N_{I,x} & N_I & 0 \\ N_{I,y} & 0 & N_I \end{bmatrix} \,. \tag{34}$$

Thus, considering arbitrary shaped elements with

$$\begin{aligned} \int\limits_{(\Omega_e)} N_{I,x} \, dA &= A_e\, N_{I,x}\,(\xi = 0, \eta = 0) \\ \int\limits_{(\Omega_e)} N_{I,y} \, dA &= A_e\, N_{I,y}\,(\xi = 0, \eta = 0) \\ \int\limits_{(\Omega_e)} N_I \, dA &\neq A_e\, N_I(\xi = 0, \eta = 0) \end{aligned} \tag{35}$$

the following result holds for an arbitrary patch only with modified shear strains according to (13), but not with (34)

$$\int\limits_{(\Omega_e)} \mathbf{B} \, dA = A_e \mathbf{B}^0 \,. \tag{36}$$

Thus, the constant stress state follows from $(31)_1$ considering (36)

$$\boldsymbol{\beta}^0 = \mathbf{C}\mathbf{B}^0\,\mathbf{v} \,. \tag{37}$$

B Appendix, Explicit representation of the one-point integrated stiffness matrix

The explicit representation of $\mathbf{k}^0_{IK} = A_e \mathbf{B}^{0T}_I \mathbf{C} \mathbf{B}^0_K$ reads

$$
\mathbf{k}^0_{IK} = \frac{1}{A_e}
\begin{bmatrix}
\begin{aligned}
& C^s_{11}\,\xi_I\xi_K \\
& + C^s_{12}\,\xi_I\eta_K \\
& + C^s_{12}\,\eta_I\xi_K \\
& + C^s_{22}\,\eta_I\eta_K
\end{aligned}
&
\begin{aligned}
& C^s_{11}b^{11}_K\,\xi_I\xi_K \\
& + C^s_{12}b^{21}_K\,\xi_I\eta_K \\
& + C^s_{12}b^{11}_K\,\eta_I\xi_K \\
& + C^s_{22}b^{21}_K\,\eta_I\eta_K
\end{aligned}
&
\begin{aligned}
& C^s_{11}b^{12}_K\,\xi_I\xi_K \\
& + C^s_{12}b^{22}_K\,\xi_I\eta_K \\
& + C^s_{12}b^{12}_K\,\eta_I\xi_K \\
& + C^s_{22}b^{22}_K\,\eta_I\eta_K
\end{aligned}
\\[2em]
\begin{aligned}
& C^s_{11}b^{11}_I\,\xi_I\xi_K \\
& + C^s_{12}b^{11}_I\,\xi_I\eta_K \\
& + C^s_{12}b^{21}_I\,\eta_I\xi_K \\
& + C^s_{22}b^{21}_I\,\eta_I\eta_K
\end{aligned}
&
\begin{aligned}
& (C^s_{11}b^{11}_I b^{11}_K + C^{b11}_{22})\,\xi_I\xi_K \\
& + (C^s_{12}b^{11}_I b^{21}_K + C^{b12}_{22})\,\xi_I\eta_K \\
& + (C^s_{12}b^{21}_I b^{11}_K + C^{b12}_{22})\,\eta_I\xi_K \\
& + (C^s_{22}b^{21}_I b^{21}_K + C^{b22}_{22})\,\eta_I\eta_K
\end{aligned}
&
\begin{aligned}
& (C^s_{11}b^{11}_I b^{12}_K + C^{b11}_{23})\,\xi_I\xi_K \\
& + (C^s_{12}b^{11}_I b^{22}_K + C^{b12}_{23})\,\xi_I\eta_K \\
& + (C^s_{12}b^{21}_I b^{12}_K + C^{b21}_{23})\,\eta_I\xi_K \\
& + (C^s_{22}b^{21}_I b^{22}_K + C^{b22}_{23})\,\eta_I\eta_K
\end{aligned}
\\[2em]
\begin{aligned}
& C^s_{11}b^{12}_I\,\xi_I\xi_K \\
& + C^s_{12}b^{12}_I\,\xi_I\eta_K \\
& + C^s_{12}b^{22}_I\,\eta_I\xi_K \\
& + C^s_{22}b^{22}_I\,\eta_I\eta_K
\end{aligned}
&
\begin{aligned}
& (C^s_{11}b^{12}_I b^{11}_K + C^{b11}_{32})\,\xi_I\xi_K \\
& + (C^s_{12}b^{12}_I b^{21}_K + C^{b12}_{32})\,\xi_I\eta_K \\
& + (C^s_{12}b^{22}_I b^{11}_K + C^{b21}_{32})\,\eta_I\xi_K \\
& + (C^s_{22}b^{22}_I b^{21}_K + C^{b22}_{32})\,\eta_I\eta_K
\end{aligned}
&
\begin{aligned}
& (C^s_{11}b^{12}_I b^{12}_K + C^{b11}_{33})\,\xi_I\xi_K \\
& + (C^s_{12}b^{12}_I b^{22}_K + C^{b12}_{33})\,\xi_I\eta_K \\
& + (C^s_{12}b^{22}_I b^{12}_K + C^{b12}_{33})\,\eta_I\xi_K \\
& + (C^s_{22}b^{22}_I b^{22}_K + C^{b22}_{33})\,\eta_I\eta_K
\end{aligned}
\end{bmatrix}
\tag{38}
$$

with

$$
\begin{aligned}
C^{b11}_{22} &= D\,(J^{02}_{22} + \tfrac{1-\nu}{2}\,J^{02}_{21}) \\
C^{b12}_{22} &= -D\,(J^0_{22}J^0_{12} + \tfrac{1-\nu}{2}\,J^0_{21}J^0_{11}) \\
C^{b22}_{22} &= D\,(J^{02}_{12} + \tfrac{1-\nu}{2}\,J^{02}_{11}) \\[1em]
C^{b11}_{33} &= D\,(J^{02}_{21} + \tfrac{1-\nu}{2}\,J^{02}_{22}) \\
C^{b12}_{33} &= -D\,(J^0_{21}J^0_{11} + \tfrac{1-\nu}{2}\,J^0_{22}J^0_{12}) \\
C^{b22}_{33} &= D\,(J^{02}_{11} + \tfrac{1-\nu}{2}\,J^{02}_{12}) \\[1em]
C^{b11}_{23} &= C^{b11}_{32} = -D\,(\tfrac{1+\nu}{2}\,J^0_{21}J^0_{22}) \\
C^{b12}_{23} &= C^{b21}_{32} = D\,(\nu J^0_{22}J^0_{11} + \tfrac{1-\nu}{2}\,J^0_{21}J^0_{12}) \\
C^{b21}_{23} &= C^{b12}_{32} = D\,(\nu J^0_{12}J^0_{21} + \tfrac{1-\nu}{2}\,J^0_{11}J^0_{22}) \\
C^{b22}_{23} &= C^{b22}_{32} = -D\,(\tfrac{1+\nu}{2}\,J^0_{11}J^0_{12})
\end{aligned}
\tag{39}
$$

$$
\begin{aligned}
C^s_{11} &= \kappa\,Gh\,(J^{02}_{22} + J^{02}_{21}) \\
C^s_{22} &= \kappa\,Gh\,(J^{02}_{11} + J^{02}_{12}) \\
C^s_{12} &= -\kappa\,Gh\,(J^0_{11}J^0_{21} + J^0_{22}J^0_{12})
\end{aligned}
$$

References

[1] Zienkiewicz, O. C., Taylor, R. L.: The Finite Element Method Vol.1–3, 5. ed., Butterworth-Heinemann, Oxford, 2000. 1, 2.2, 3

[2] Batoz J. L., Tahar M. B.: Evaluation of a New Quadrilateral Thin Plate Bending Element, Int. J. Num. Meth. Engng. 21, 1655–1677, 1982. 1, 3.1, 3.2.1, 3.2.2, 3.4.2, 3.5

[3] Reissner, E.: The effect of transverse shear deformation on the bending of elastic plates, J. Appl. Mech. 12, 69–76, 1945. 1, 3.5

[4] Mindlin, R.D.: Influence of rotatory inertia and shear flexural motions of isotropic elastic plates, J. Appl. Mech. 18, 31–38, 1951. 1

[5] Timoshenko, S. P., Woinowsky–Krieger, S.: Theory of Plates and Shells, McGraw–Hill 2^{nd}ed, 1970. 1, 3.2.1, 3.2.2

[6] Zienkiewicz, O. C., Taylor, R.L., Too, J.M.: Reduced integration techniques in general analysis of plates and shells, Int. J. Num. Meth. Engng., 3, 275–290, 1971. 1

[7] Hughes, T. R. J., Taylor, R. L., Kanoknukulchai, W.: A simple and efficient finite element for plate bending, Int. J. Num. Meth. Engng., 11, 1529–1543, 1977. 1, 3.5

[8] Belytschko, T., Tsay, C.-S.: A stabilization procedure for the quadrilateral plate element with one–point quadrature, Int. J. Num. Meth. Engng., 19, 405–419, 1983. 1, 3.1, 3, 3.2.2, 3.4.1, 3.4.2, 3.5, 3.5

[9] Belytschko, T., Bachrach, W.: Efficient implementation of quadrilaterals with high coarse–mesh accuracy, Comp. Meth. Appl. Mech. Engng., 54, 279–301, 1986. 1

[10] Reese, S., Wriggers, P.: A stabilization technique to avoid hourglassing in finite elasticity, Int. J. Num. Meth. Engng., 48, 79–109, 2000. 1

[11] MacNeal, R. H.: A simple quadrilateral shell element, Comput. Struct., 8, 175–183, 1978. 1

[12] Hughes, T. J. R. and Tezduyar, T. E.: Finite elements based upon Mindlin plate theory, with particular reference to the 4–node bilinear isoparametric element, J. Appl. Mech., 48, 587–595, 1981. 1

[13] MacNeal, R. H.: Derivation of element stiffness matrices by assumed strain distribution, Nuclear Engineering Design, 70, 3–12, 1982. 1

[14] Dvorkin, E., Bathe, K.-J.: A Continuum Mechanics Based Four Node Shell Element for General Nonlinear Analysis, Engineering Computations, 1, 77–88, 1984. 1, 2.2

[15] Bathe, K.J., Dvorkin, E.: A 4–Node Plate Bending Element based on Mindlin/Reissner Theory and a Mixed Interpolation, Int. J. Num. Meth. Engng., 21, 367–383, 1985. 1, 3.2.1, 3.2.2, 3.3, 3.4.2

[16] Hinton, E. and Huang, H. C.: A family of quadrilateral Mindlin plate elements with substitute shear strain fields. Comp. Struct., 23, 409–431, 1986. 1

[17] Oñate, E., Zienkiewicz, O. C., Suárez, B. and Taylor, R. L.: A general methodology for deriving shear constrained Reissner–Mindlin plate elements, Int. J. Num. Meth. Engng., 33, 345–367, 1992. 1

[18] Kebari, H.: A one point integrated assumed strain 4–node Mindlin plate element, Engineering Computations, 7, 284–290, 1990. 1

[19] Batoz, J. L. and Lardeur, P.: A discrete shear triangular nine D.O.F. element for the analysis of thick to very thin plates, Int. J. Num. Meth. Engng., 28, 533–560, 1989. 1

[20] Pian, T. H. H., Kang, D. and Wang, C.: Hybrid plate elements based on balanced stresses and displacements, Finite Element Methods for Plate and Shell Structures, Vol. 1, Pineridge Press, Swansea, 244–265, 1986. 1

[21] Saleeb, A. F. and Chang, T. Y.: An efficient quadrilateral element for plate bending analysis, Int. J. Num. Meth. Engng., 24, 1123–1155, 1987. 1, 2.2, 3.2.2, 3.2.2

[22] Baumann, M., Schweizerhof K., Andrussow S.: An efficient mixed hybrid 4-node shell element with assumed stresses for membrane, bending and shear parts, Engineerung Computations, 11, 69–80 , 1994. 1, 2.2

[23] Taylor, R. L., Simo, J. C., Zienkiewicz, O. C., Chan, A. C. H.: The patch test - A condition for assessing FEM convergence, Int. J. Num. Meth. Engng., 22, 39–62, 1986. 2.2

[24] Pian, T. H. H. and Sumihara, K.: Rational approach for assumed stress finite elements. Int. J. Num. Meth. Eng., 20, 1685-1695, 1984. 2.2

[25] Lee, S. L., Ballesteros, P.: Uniformly loaded rectangular plate supported at corners, Int. J. Mech. Sci., 2, 206–211, 1960. 3.4.1

[26] Leissa, A. W.: Vibration of plates, NASA SP-160, 1969. 3.4.2